Supporting Information

Dealloying $PdBi_2$ Nanoflakes to Palladium Hydride Leads to Enhanced Electrocatalytic N_2 Reduction

Nikolas Antonatos[1,], Joshua D. Elliott[2], Vlastimil Mazánek[1], Petr Marvan[1], Paola Carbone[2], Weixiang Geng[3], Yu Jing[3], Zdeněk Sofer[1,*]*

[1] Department of Inorganic Chemistry, University of Chemistry and Technology Prague, Technická 5, 166 28 Prague 6, Czech Republic; e-mail: zdenek.sofer@vscht.cz ; nikolaoa@vscht.cz

[2] Department of Chemical Engineering and Analytical Science, University of Manchester, Manchester M13 9PL, United Kingdom

[3] Jiangsu Co-Innovation Centre of Efficient Processing and Utilization of Forest Resources, International Innovation Center for Forest Chemicals and Materials, College of Chemical Engineering, Nanjing Forestry University, Nanjing 210037, China

Table S1. The complete spectrum of Raman active mode frequencies and symmetries computed from PBE-SOC DFPT simulations of α-$PdBi_2$.

Frequency (cm^{-1})	Symmetry	Frequency (cm^{-1})	Symmetry
16.2	A_g	75.5	A_g
20.3	B_g	79.0	A_g
34.0	A_g	96.5	A_g
44.6	B_g	116.9	A_g
44.8	A_g	120.6	A_g
63.7	A_g	127.1	B_g
64.1	A_g	127.6	A_g
68.3	B_g	147.8	A_g
69.9	B_g	158.3	B_g

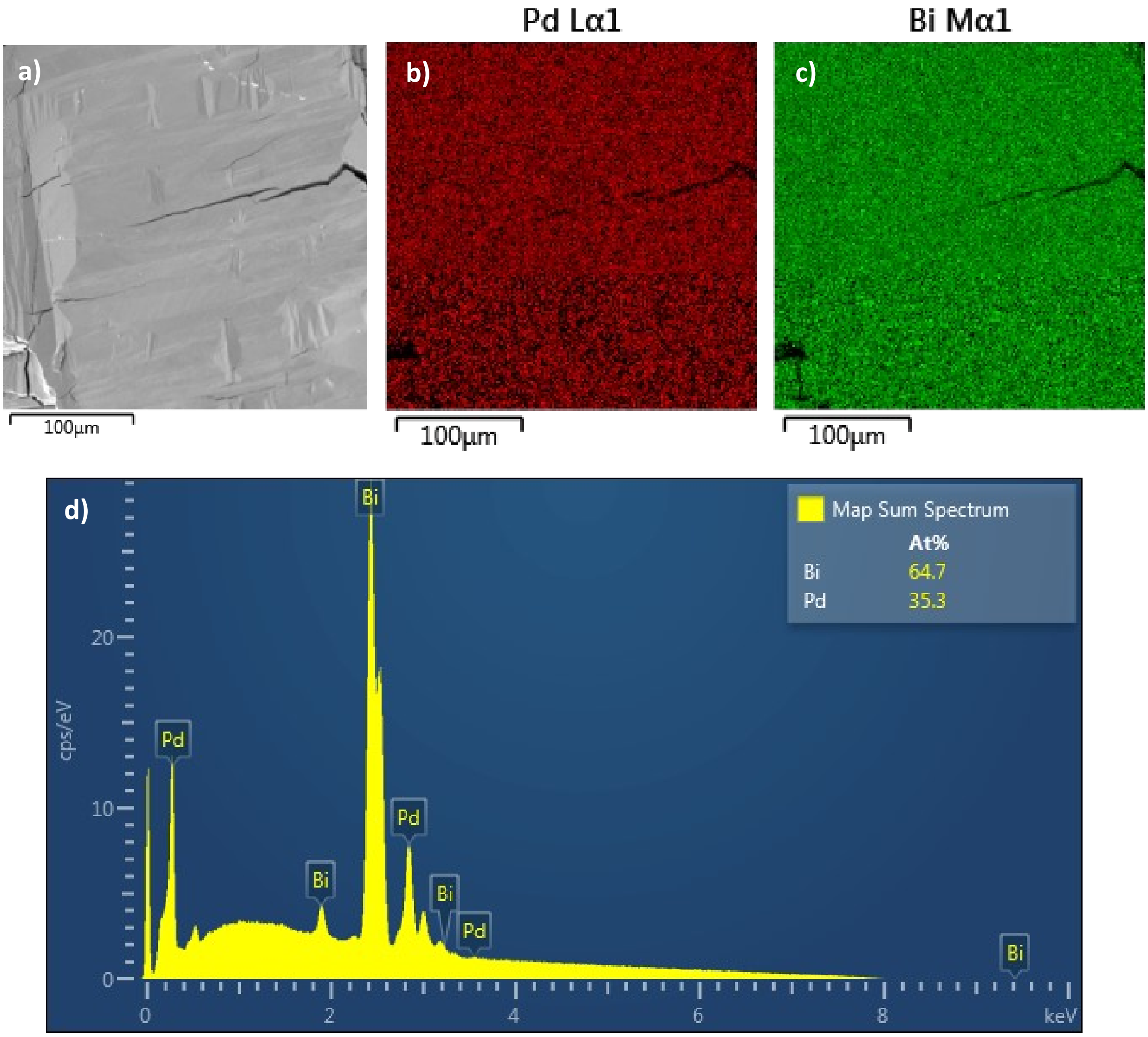

Figure S1. a) SEM image of bulk $PdBi_2$ with the corresponding EDS elemental maps of **b)** palladium and **c)** bismuth. **d)** EDS map spectrum of $PdBi_2$ depicting the ratio of Pd:Bi at 1:2.

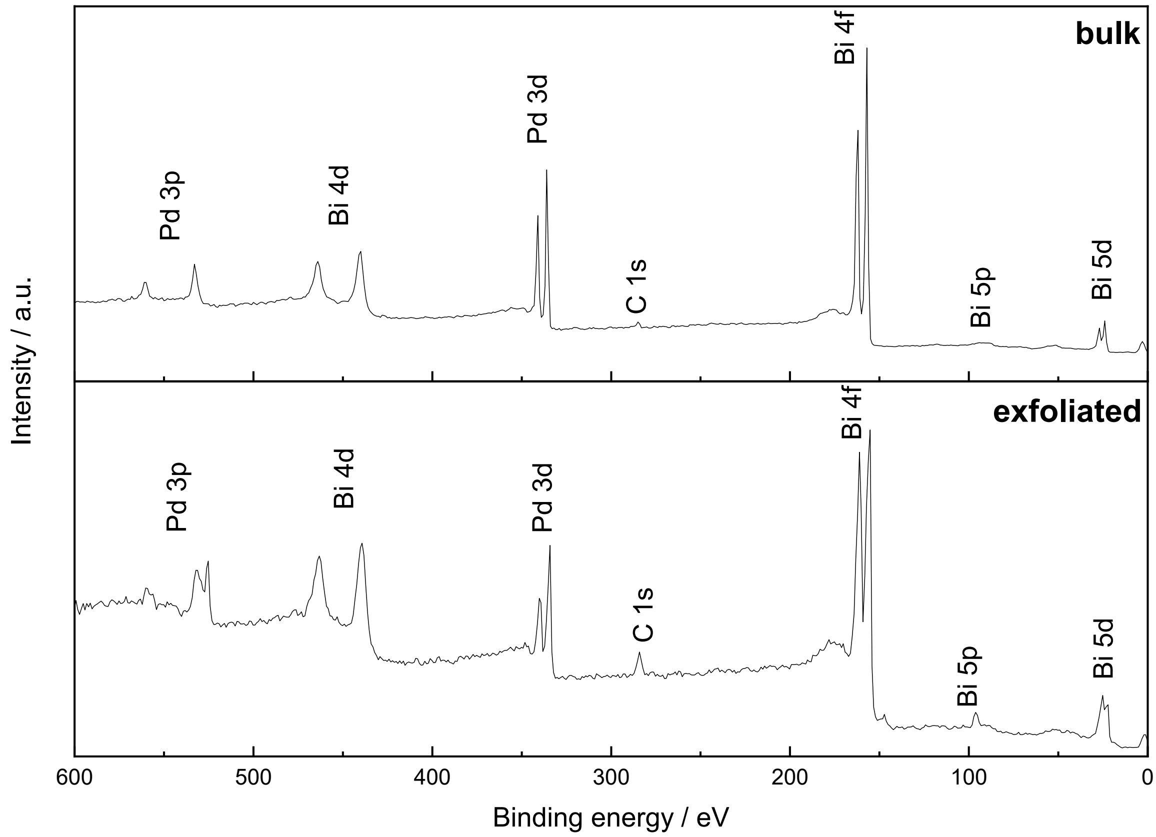

Figure S2. Wide survey XPS spectra of bulk and exfoliated $PdBi_2$.

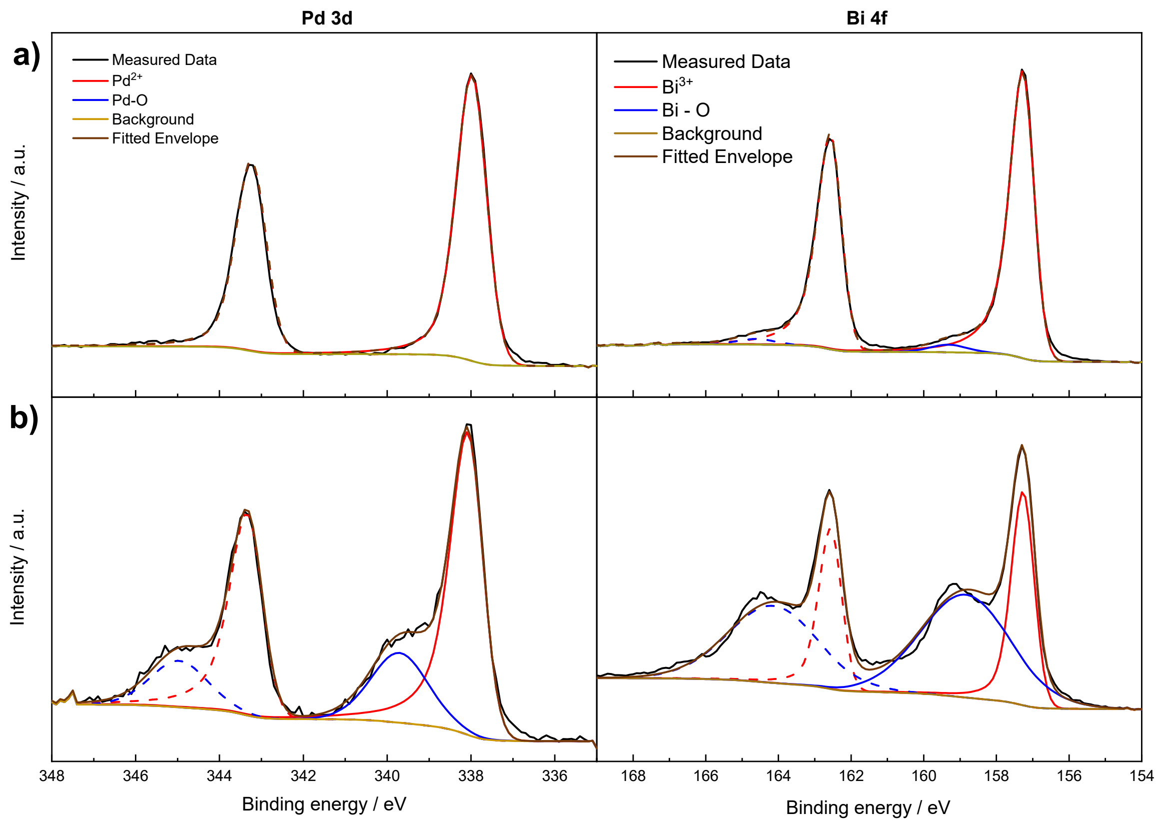

Figure S3. High-resolution XPS spectra of Pd 3d and Bi 4f of **a)** bulk and **b)** exfoliated $PdBi_2$.

Table S2. Ammonia formation rates and Faradaic efficiencies of exfoliated $PdBi_2$ nanoflakes at different potentials.

Potential vs. Ag/AgCl / V	NH_3 yield / $\mu g\ cm^{-2}\ h^{-1}$	Faradaic efficiency
-1.4	4.33	3.16
-1.5 (1)	24.20	4.71
-1.5 (2)	20.38	4.08
-1.5 (3)	22.17	4.30
-1.5 average	22.25 ± 1.56	4.36 ± 0.26
-1.6 (1)	28.03	2.39
-1.6 (2)	26.75	2.01
-1.6 average	27.39 ± 0.64	2.20 ± 0.19
-1.7 (1)	29.81	0.66
-1.7 (2)	28.28	0.61
-1.7 average	29.04 ± 0.76	0.64 ± 0.03

Table S3. Ammonia formation rates and Faradaic efficiencies of exfoliated $PdBi_2$ nanoflakes after each NRR cycle at -1.5 V vs. Ag/AgCl.

Cycle number	NH_3 yield / $\mu g\ cm^{-2}\ h^{-1}$	Faradaic efficiency
1	23.44	4.52
2	25.99	7.37
3	30.32	14.87
4	28.53	13.88
5	31.34	16.98

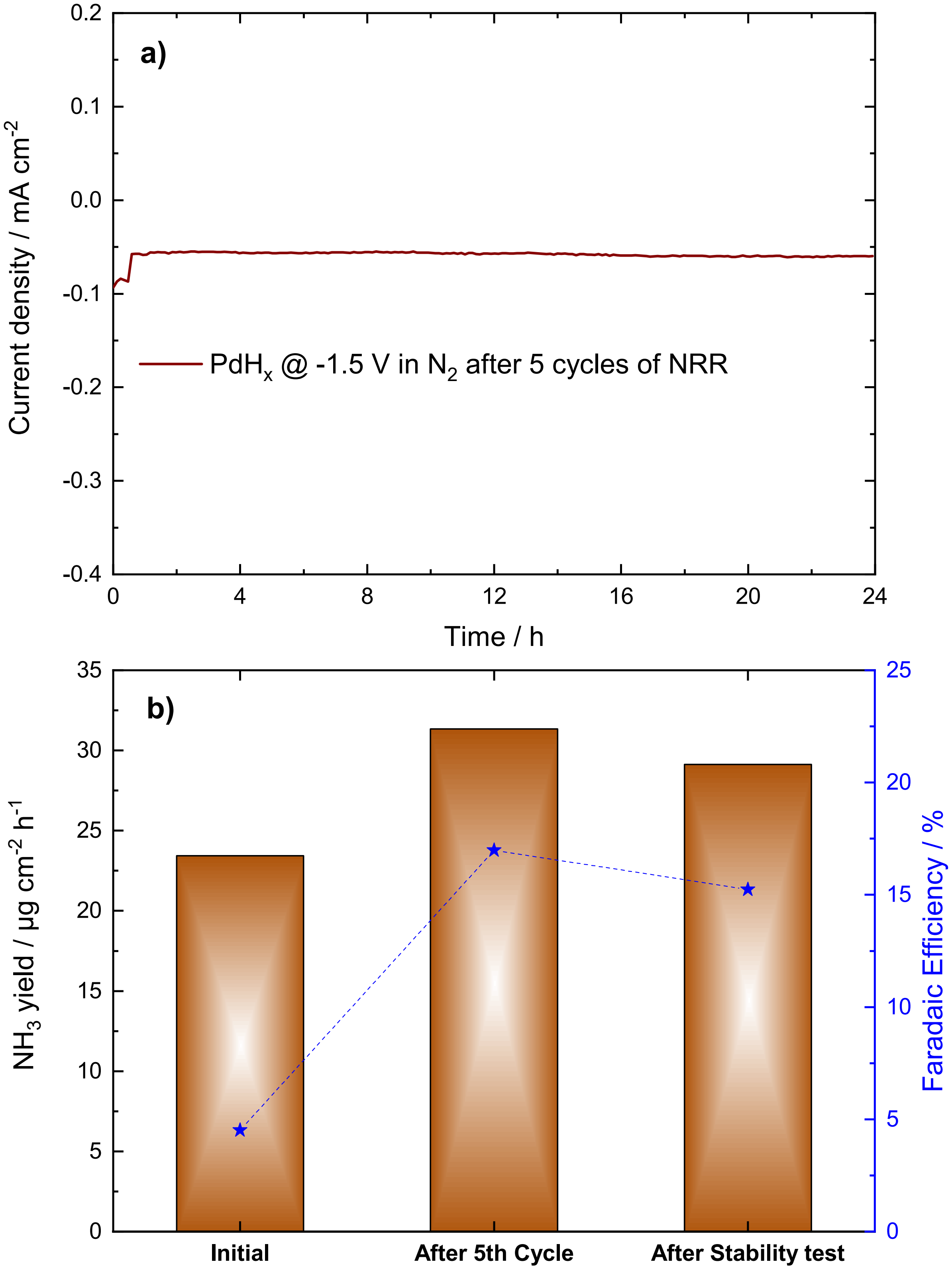

Figure S4. a) Long-term choronoamperometry curve of PdH_x showing good stability. **b)** NH_3 yield and FE for initial, after 5 cycles of NRR and post-stability test NRR (after 24 h) of $PdBi_2$ at -1.5 V vs. Ag/AgCl.

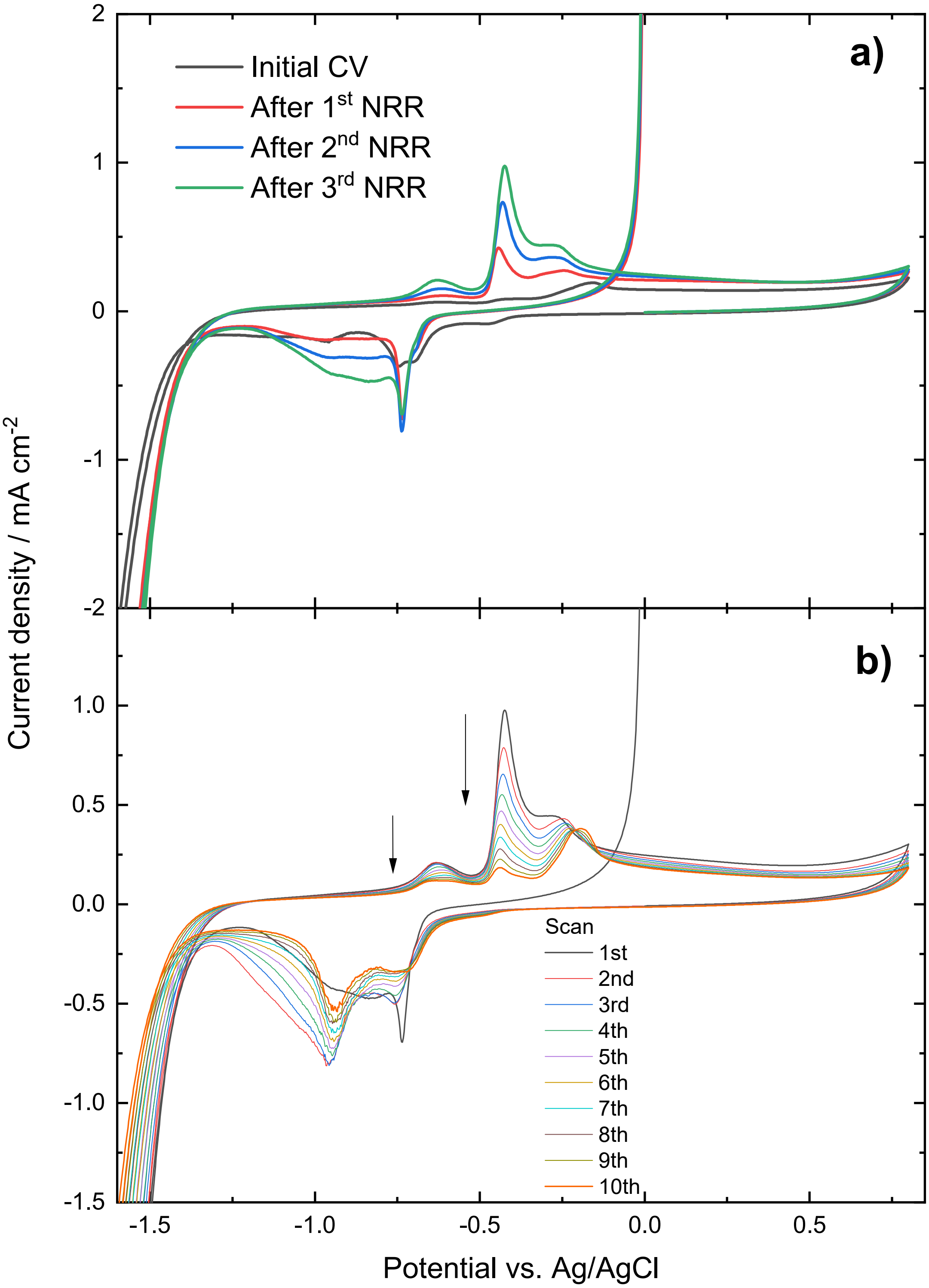

Figure S5. a) First CV of $PdBi_2$, before any catalysis and after one, two and three NRR cycles. **b)** Ten consecutive CVs of $PdBi_2$, after three cycles of NRR. Scan rate: 100 mV s^{-1}.

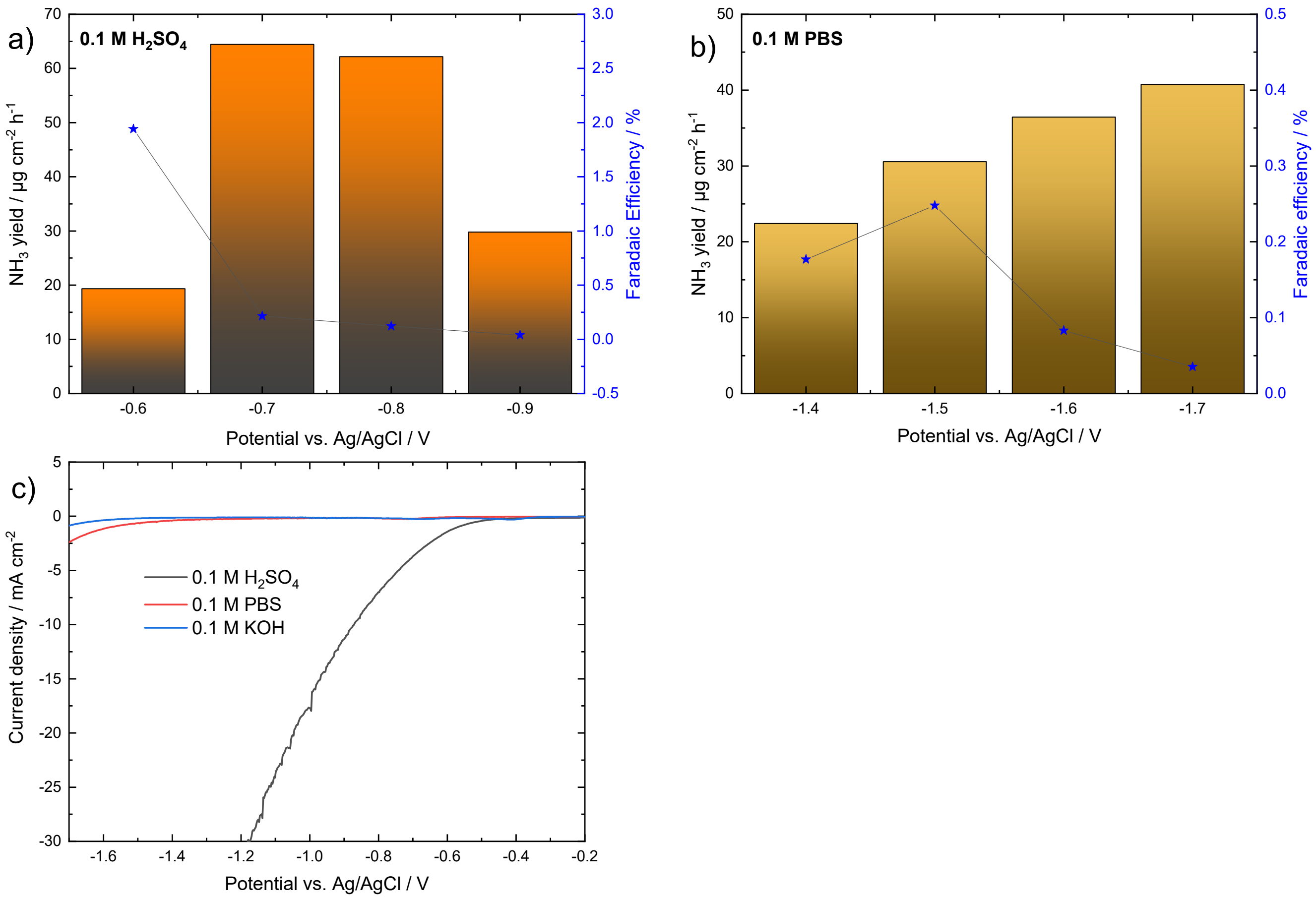

Figure S6. NH_3 formation rate of $PdBi_2$ with corresponding Faradaic efficiency in **a)** acidic environment (0.1 M H_2SO_4, pH = 1) and **b)** neutral environment (0.1 M PBS, pH = 7). **c)** LSV curves of $PdBi_2$ in different electrolytes. Scan rate: 100 mV s^{-1}.

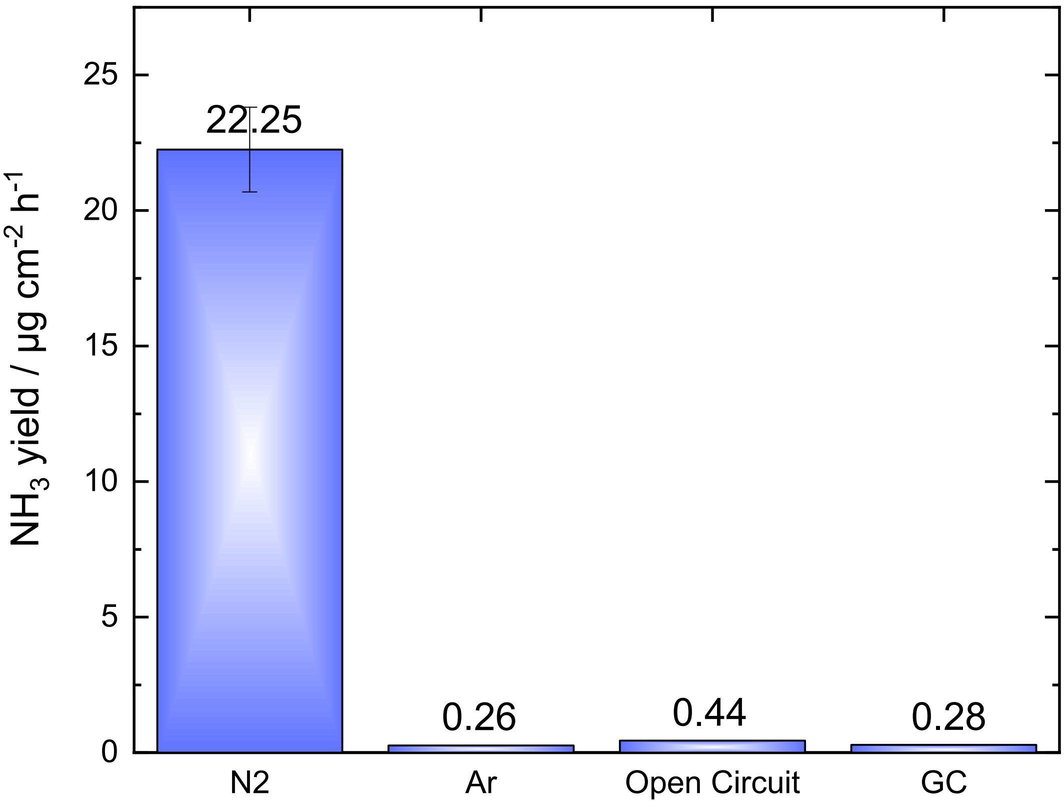

Figure S7. NH3 yield comparison in 0.1 M KOH between: PdBi2 in saturated N2 at -1.5 V, PdBi2 in saturated Ar at -1.5 V, PdBi2 in saturated N2 at OCP and bare GC in saturated N2 at -1.5 V.

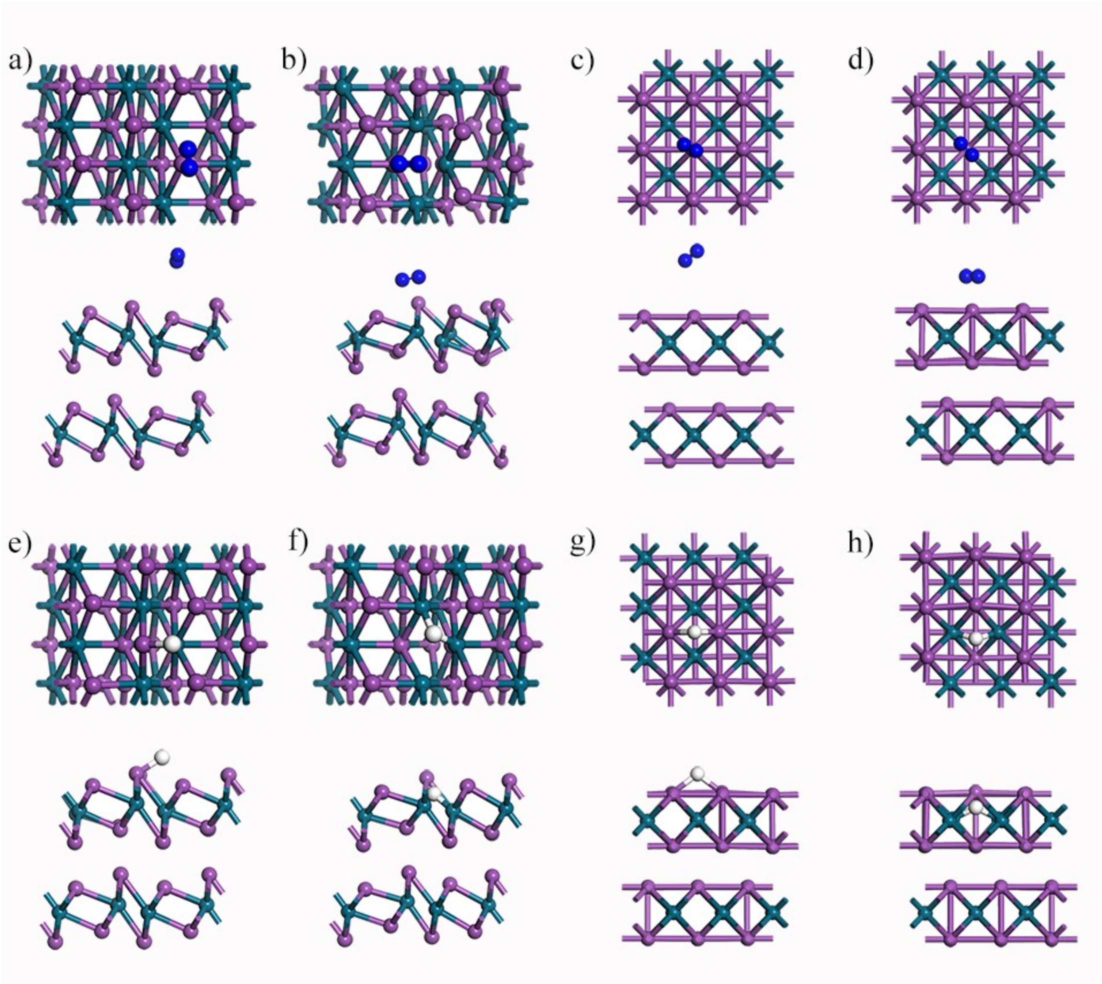

Figure S8. Schematics from the top and side views for the adsorption of H and N_2 on different phases of $PdBi_2$ without or with Bi vacancies. (a) α-$PdBi_2$-N_2, (b) α-$PdBi_2$-v-N_2, (c) β-$PdBi_2$-N_2, (d) β-$PdBi_2$-v-N_2, (e) α-$PdBi_2$-H, (f) α-$PdBi_2$-v-H, (g) β-$PdBi_2$-H and (h) β-$PdBi_2$-v-H.

Table S4. The adsorption energy (E_{ad}) and distance ($D_{ad\text{-}M}$) between the adsorbed species and the adsorption site of α-$PdBi_2$, α-$PdBi_2$-v, β-$PdBi_2$ and β-$PdBi_2$-v.

	α-$PdBi_2$	**α-$PdBi_2$-v**	**β-$PdBi_2$**	**β-$PdBi_2$-v**
E_{ad} (H) / eV	0.50	0.25	0.75	0.29
E_{ad} (N_2) / eV	-0.08	-0.17	-0.09	-0.15
$D_{H\text{-}M}$ / Å	1.89	1.77	2.13	1.78
$D_{N2\text{-}M}$ / Å	3.93	3.80	3.89	3.73

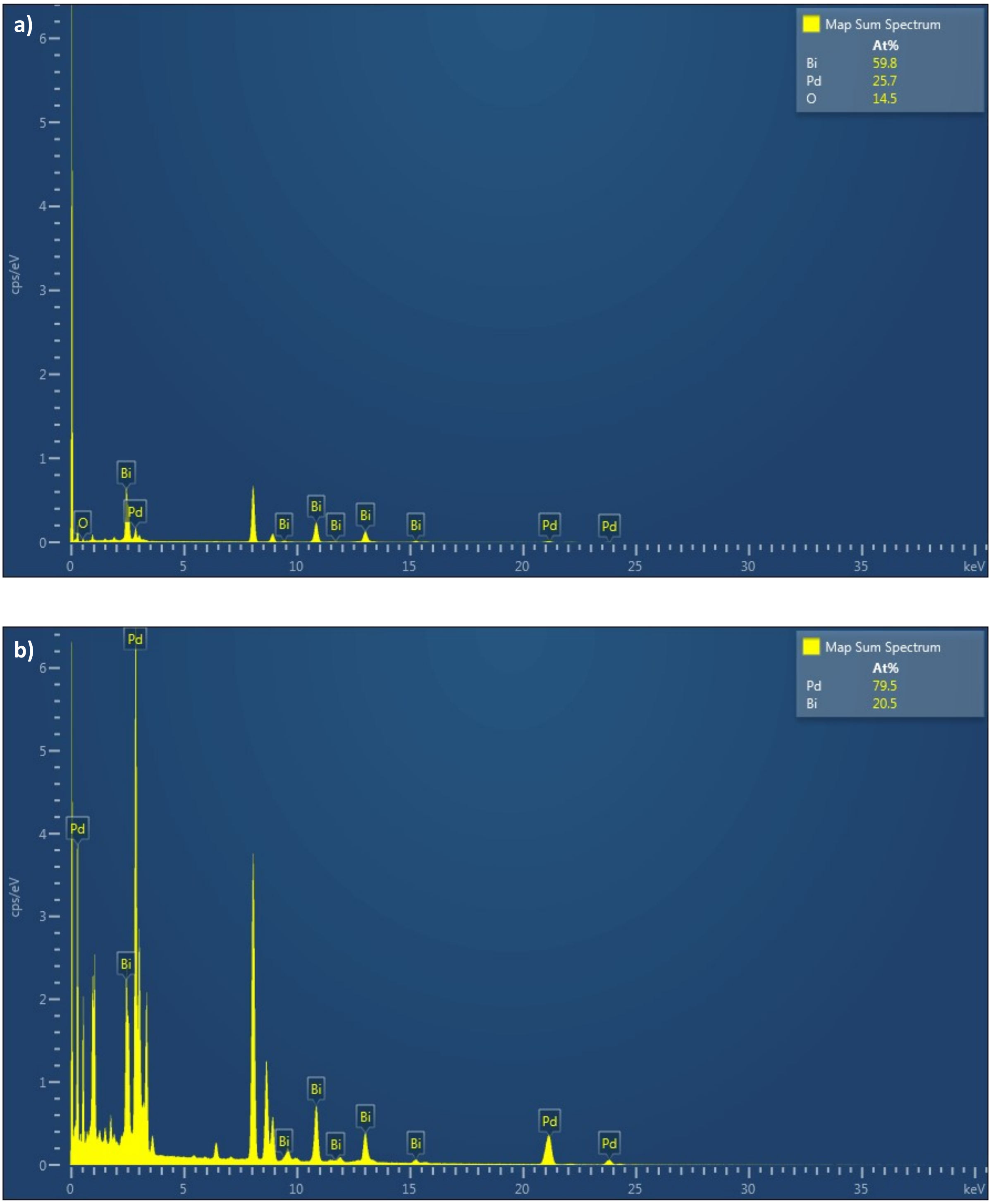

Figure S9. TEM/EDS map spectra of exfoliated $PdBi_2$ flakes **a)** before and **b)** after NRR depicting the change of Pd:Bi ratio from 1:2 to 4:1. Peaks appearing around 8 keV are due to the Cu of the TEM grids.

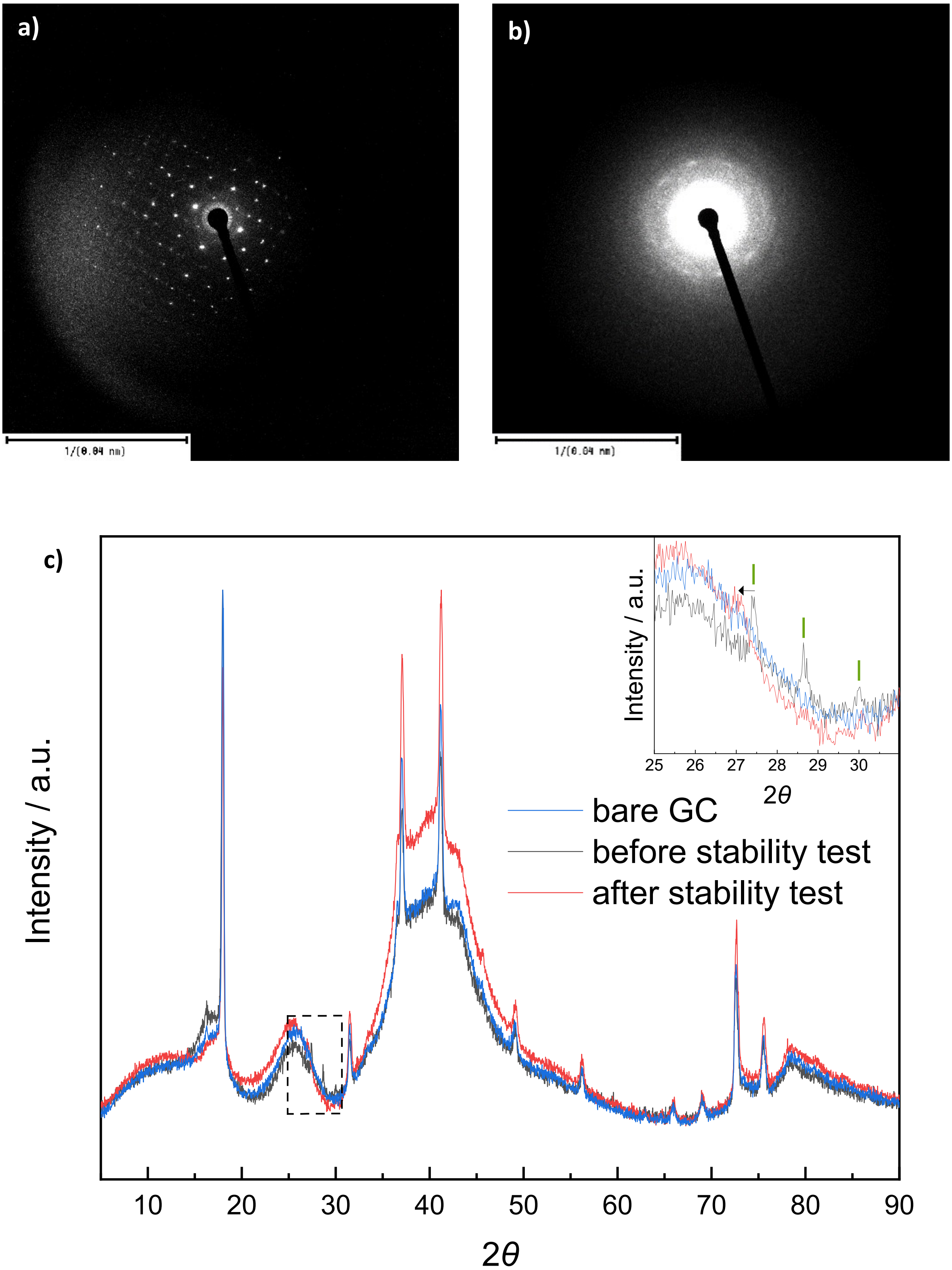

Figure S10. TEM/SAED diffraction patterns of exfoliated $PdBi_2$ **a)** before and **b)** after the NRR stability test. **c)** XRD patterns of bare GC and $PdBi_2$ on GC before and after the NRR stability test. The inset graph depicts the enlarged frame.

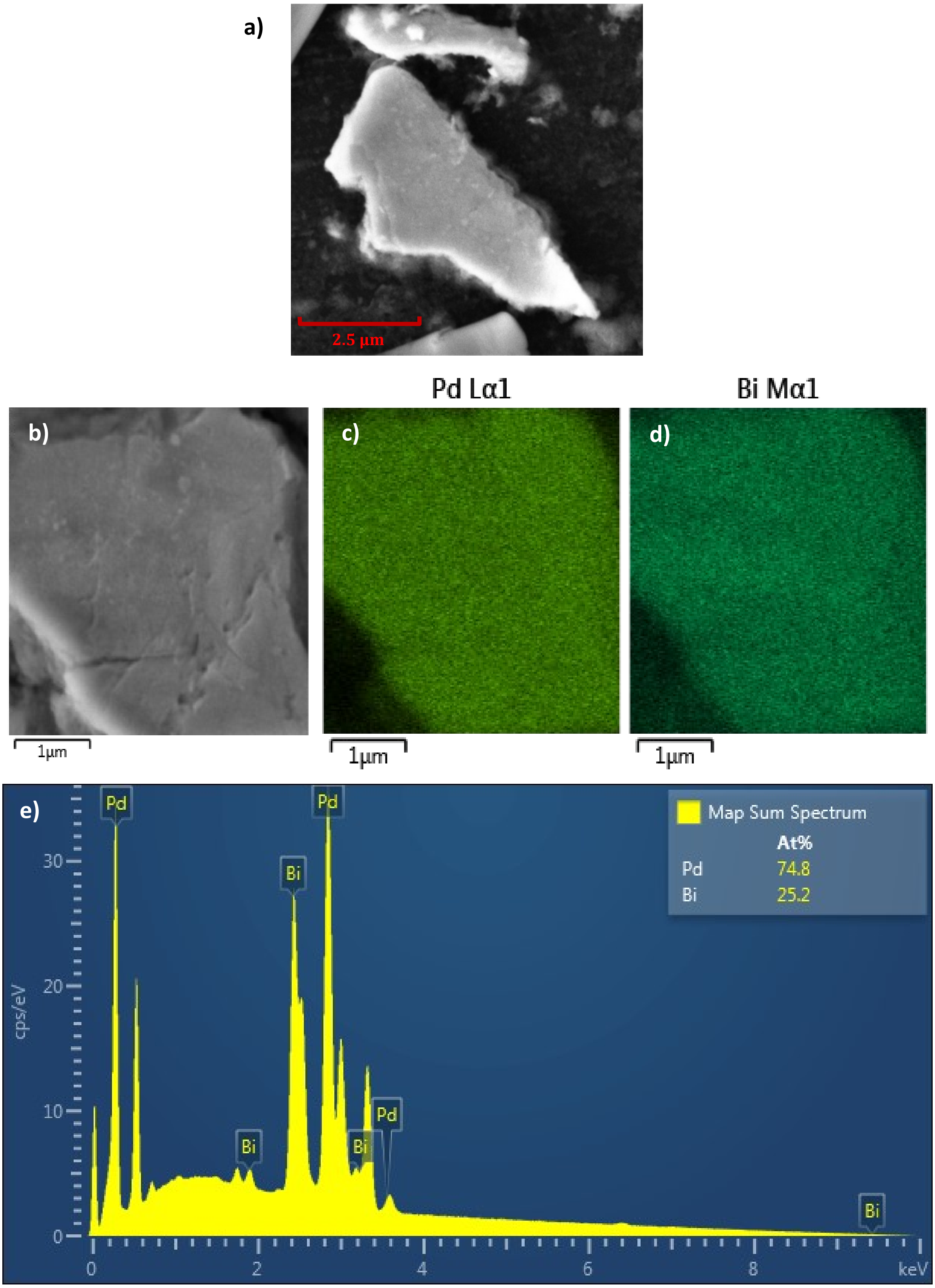

Figure S11. a-b) SEM images of exfoliated $PdBi_2$ after a 24-hour stability test with the corresponding EDS elemental maps of **c)** palladium and **d)** bismuth. **e)** EDS map spectrum of $PdBi_2$ depicting the ratio of Pd:Bi at 3:1.

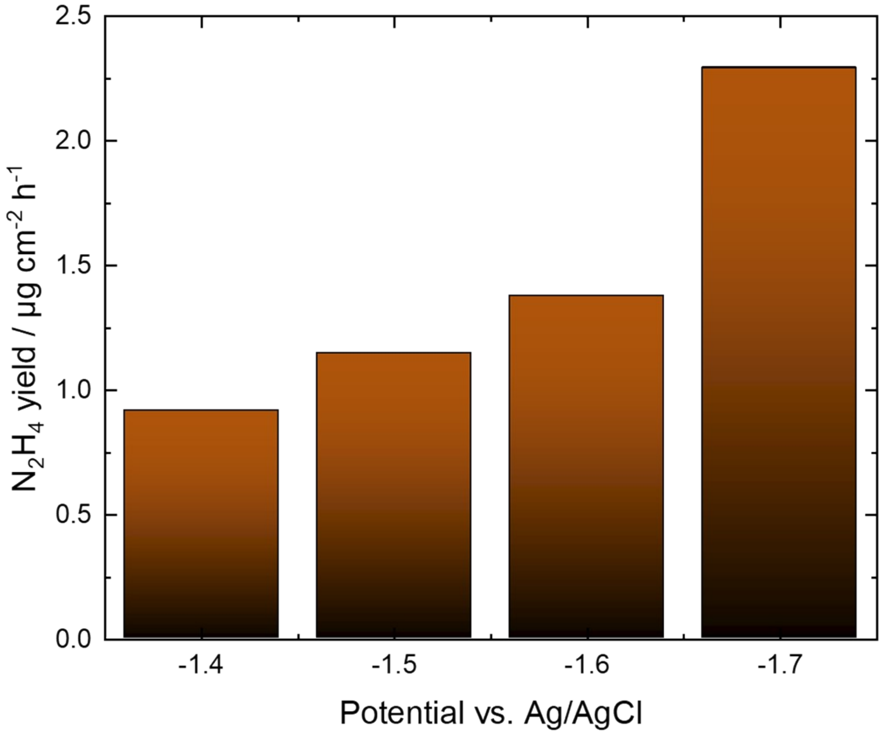

Figure S12. N_2H_4 formation rate of exfoliated $PdBi_2$ at different potentials.

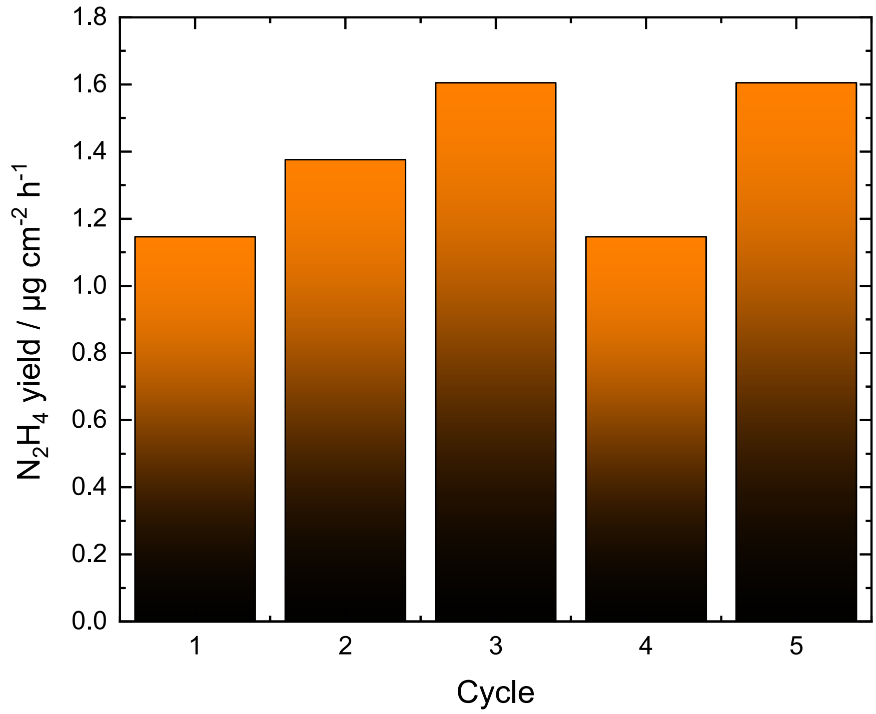

Figure S13. N_2H_4 formation rate of dealloyed $PdBi_2$ flakes of 2 h cycles at -1.5 V vs. Ag/AgCl.

Construction of theoretical Pourbaix diagram for $PdBi_2$

In this supplementary section we report the reactions involved in the construction of the theoretical Pourbaix diagram,[1] details are provided for the Pd-only, Bi-only, and mixed reactions. Furthermore, we also provide a set of tables that report on DFT formation energies and the experimentally motivated corrections to those energies.

For reactions involving Pd-based reagents, we establish the Pd^{2+} ion as the standard reference for the calculation of reaction free energies. Thus, we consider the following reactions:

$$Pd^{2+} \rightleftharpoons Pd^{2+} \#(1)$$

$$Pd^{2+} + 2e^{-} \rightleftharpoons Pd\#(2)$$

$$Pd^{2+} + H_2O \rightleftharpoons PdO + 2H^{+} \#(3)$$

$$Pd^{2+} + 2H_2O \rightleftharpoons PdO_2 + 4H^{+} + 2e^{-} \#(4)$$

Similarly, we adopt the Bi^{3+} ion as a standard reference for calculation of the free energy in reactions involving Bi-based reagents. These reactions are as follows:

$$Bi^{3+} \rightleftharpoons Bi^{3+} \#(5)$$

$$Bi^{3+} + 3e^{-} \rightleftharpoons Bi\#(6)$$

$$Bi^{3+} + 3H^{+} + 6e^{-} \rightleftharpoons BiH_3\#(7)$$

$$Bi^{3+} + H_2O \rightleftharpoons BiO^{+} + 2H^{+} \#(8)$$

$$Bi^{3+} + {}^{3}/_{2}H_2O \rightleftharpoons {}^{1}/_{2}Bi_2O_3 + 3H^{+} \#(9)$$

$$Bi^{3+} + {}^{7}/_{4}H_2O \rightleftharpoons {}^{1}/_{4}Bi_4O_7 + {}^{7}/_{2}H^{+} + {}^{1}/_{2}e^{-} \#(10)$$

A two metals diagram was constructed following the procedure outlined in the work of Cubicciotti, to this end the Pd metal was chosen as the primary component. Assuming that each

[1]K.A. Persson, B. Waldwick, P. Lazic and G. Ceder, *Phys. Rev. B,* 2012, **85,** 235438

stable Bi species exhibits a constant activity, the reactions considered for the formation of $PdBi_2$ are:

$$Bi^{3+} + {}^{1}/_{2}Pd^{2+} + 4e^{-} \rightleftharpoons PdBi_2 \#(11)$$

$$Bi^{3+} + {}^{1}/_{2}Pd + 3e^{-} \rightleftharpoons PdBi_2 \#(12)$$

$$Bi^{3+} + {}^{1}/_{2}PdO + H^{+} + 4e^{-} \rightleftharpoons PdBi_2 + {}^{1}/_{2}H_2O \#(13)$$

$$Bi^{3+} + {}^{1}/_{2}PdO_2 + 2H^{+} + 5e^{-} \rightleftharpoons PdBi_2 + H_2O \#(14)$$

The theoretical free energy of formation (ΔG_f^{DFT}), computed at the PBE-SOC level of theory for each of the solid-state species are reported in the following table:

Table S5. Theoretical free energy of formation of each of the solid species considered in the construction of the Pourbaix diagram.

Solid	ΔG_f^{DFT} (eV)
$PdBi_2$	-0.760
PdO	-1.177
PdO_2	-0.255
Pd	0.000
Bi_2O_3	-5.232
Bi_4O_7	-10.511
Bi	0.000

The corrections applied to the experimental ion chemical potentials based on the computed formation free energies was -0.098 eV for Bi^{3+} and BiO^{+} ions and -0.513 eV for the Pd^{2+} ion.[2]

[2] M. Pourbaix, Atlas of Electrochemical Equilibria in Aqueous Solutions; 2nd Ed.: National Association of Corrosion Engineers, Houston, Texas, **1974**